Coating Optimization

ET-0006A-14

I. M. Pinto and the UniSannio ELiTES Team

on behalf of ELiTES WP2

Coating Optimization

I.M. Pinto and the UniSannio ELiTES Team

1.1 Coating Noises

Random fluctuations in the optical length of the arm-cavities of Michelson interferometer based gravitational wave (GW) detectors may originate from several thermal noise mechanisms (Rao, 2003), including[1]: Brownian noise in the mirror substrates (Levin et al., 1998), and the mirror coatings (Crooks et al., 2002), temperature-fluctuations driven noises, mediated by thermal expansion (thermoelastic noise) in the mirror substrates (Liu and Thorne, 2000) and coatings (Braginsky and Vyatchanin, 2003), by the dependence on temperature of the refractive index of the coating materials (coating thermorefractive noise (Braginsky et al., 2000)), and eventually by the thermal dependence of all material constants involved (see Ch. 3 in (Harry et al, 2012) for a comprehensive review). Temperature fluctuations include, in principle, both intrinsic ("thermodynamic"), and exogenous ("photothermal") components, due to fluctuations in the power absorbed by lossy dielectrics (Braginsky et al., 1999).
The relative weight of the various noise terms in a typical advanced detector (Advanced LIGO) using the standard quarter-wavelength coatings is illustrated in Figure 0, for the specific case of Advanced LIGO based on presently available estimates of the relevant material properties.
Coating Brownian noise represents to date the main contribution to the coating noise budget, and is expected to set the noise floor of present and next-generation (advanced) interferometric detectors of GW.
The visibility distance of gravitational wave antennas is proportional to the reciprocal square root of the noise power spectral density (henceforth PSD). Thus a mere 10% reduction in the PSD level corresponds to a $\sim 17\%$ increase in the visibility volume, and hence in the observable event rate (under the simplest assumption where potential gravitational wave sources are distributed homogeneously and isotropically).
This chapter is focused on design strategies for minimizing Brownian (and more generally, thermal) noise in high-reflectivity optical coatings. It is organized as follows: Brownian noise formulas are the subject of Sect. 1.2. Section 1.3 presents the key ideas of coating design optimization aimed at minimizing Brownian noise for a prescribed reflectance. Extension to dichroic mirrors is worked out in Sect. 1.4 . Thermo-optic and thermoelastic noises are reviewed in Sect. 1.5, with a discussion of pertinent minimization criteria. Section 1.6 collects the needed formulas for describing the optical properties of dielectric coatings.

1.2 Coating Brownian Noise

For coatings using only two different materials (binary coatings), the (frequency dependent) power spectral density (henceforth PSD) of Brownian noise induced random fluctuations of the mirror front face in the normal ($\hat{z}$) direction was first

[1] Historically, these different noises entered the stage at different times, and were studied separately. An appealing *ab initio* calculation of coating noise including all these terms (and their possible correlations) has been recently proposed in (Gurkovski and Vyatchanin, 2010)

deduced in (Harry et al., 2002) via the fluctuation-dissipation theorem (Kubo, 1966), and reads

$$S_z^{(B)}(f) = \frac{2k_BT}{\pi^{3/2}f}\frac{1-\sigma^2}{wY}\phi_c, \tag{1.1}$$

where:

$$\begin{aligned}\phi_c = \frac{d_1+d_2}{\sqrt{\pi}w}\frac{1}{Y_\perp}\Bigg\{&\left[\frac{Y}{1-\sigma^2} - \frac{2\sigma_\perp^2 Y Y_\parallel}{Y_\perp(1-\sigma^2)(1-\sigma_\parallel)}\right]\phi_\perp \\ &+ \frac{Y_\parallel\sigma_\perp(1-2\sigma)}{(1-\sigma_\parallel)(1-\sigma)}(\phi_\parallel - \phi_\perp) \\ &+ \frac{Y_\parallel Y_\perp(1+\sigma)(1-2\sigma)^2}{Y(1-\sigma_\parallel^2)(1-\sigma)}\phi_\parallel\Bigg\}\end{aligned} \tag{1.2}$$

is the coating loss angle. In (1.1),(1.2) k_B is Boltzmann's constant, T the absolute temperature, w the laser beam width[2], d_1 and d_2 are the total thicknesses of the two materials, ϕ, Y and σ the mechanical loss angle, Young modulus and Poisson ratio, pertinent to the substrate (no suffix), and to the coating under parallel (suffix $\parallel$) and perpendicular (suffix $\perp$) stresses[3]. The quantities in (1.2) were computed in (Harry et al., 2004) as[4].

$$\begin{cases} Y_\perp = \dfrac{d_1+d_2}{Y_1^{-1}d_1 + Y_2^{-1}d_2} \\ Y_\parallel = \dfrac{Y_1d_1 + Y_2d_2}{d_1+d_2} \\ \phi_\perp = Y_\perp\left(\dfrac{Y_1^{-1}\phi_1 d_1 + Y_2^{-1}\phi_2 d_2}{d_1+d_2}\right) \\ \phi_\parallel = Y_\parallel^{-1}\left(\dfrac{Y_1\phi_1 d_1 + Y_2\phi_2 d_2}{d_1+d_2}\right), \end{cases} . \tag{1.3}$$

It is readily seen that letting

$$\tilde{Y}_i = Y_i(1-\imath\phi_i) \tag{1.4}$$

[2]The normalized beam intensity profile for a Gaussian beam is

$$\mathcal{I}(r) = \frac{2}{\pi w^2}\exp\left(\frac{-2r^2}{w^2}\right).$$

Occasionally, the beam radius $r_0 = w/\sqrt{2}$ is used in the Technical Literature.

[3]Note that the denominator in the first term in brackets multiplying $\phi_\perp$ in (1.2) appears as $1-\sigma_\perp^2$ in (Harry et al., 2004, eq. (8)), and as $1-\sigma_\perp$ in (Harry et al., 2006, eq. (3)). The correct formula used here is given in (Harry et al., 2002, eq. (2)), and is consistent with the limiting form reported in (Harry et al., 2002, eq. (21)) for $Y_\parallel = Y_\perp = Y$.

[4]Note that the equation for $\phi_\parallel$ in (1.3) is mis-written in (Harry et al., 2006), where eq. (8) entails an obvious dimensional error.

where $\tilde{Y}_i$ is the complex Young modulus, Y_i its real part, and ϕ_i the mechanical loss angle (assumed $\ll 1$), eq.s (1.3) are obtained taking the real part and the argument of

$$\tilde{Y}_\perp = \langle \tilde{Y}_i \rangle_R, \ \tilde{Y}_\parallel = \langle \tilde{Y}_i \rangle_V \tag{1.5}$$

where $\langle \cdot \rangle_{R,V}$ denote the Reuss (isostress) and Voigt (isostrain) mixture-averages, respectively (see, e.g., Lakes, 2009).
The Poisson ratios, on the other hand, may be computed from (Harry et al., 2004)

$$\sigma_\perp = \frac{\sigma_1 Y_1 d_1 + \sigma_2 Y_2 d_2}{Y_1 d_1 + Y_2 d_2} \tag{1.6}$$

and taking the (only) positive root of the quadratic equation ((Harry et al., 2004), eqs. (3) and (15)):

$$\frac{\sigma_1 Y_1 d_1}{(1+\sigma_1)(1-2\sigma_1)} + \frac{\sigma_2 Y_2 d_2}{(1+\sigma_2)(1-2\sigma_2)} = -\frac{Y_\parallel(\sigma_\perp^2 Y_\parallel + \sigma_\parallel Y_\perp)(d_1+d_2)}{(\sigma_\parallel+1)[2\sigma_\perp^2 Y_\parallel - (1-\sigma_\parallel)Y_\perp]}. \tag{1.7}$$

The limiting form of eqs. (1.2) for vanishingly small Poisson ratios is remarkably simple [5]:

$$\phi_c = \frac{d_1 + d_2}{\sqrt{\pi} w} \left(\frac{Y}{Y_\perp} \phi_\perp + \frac{Y_\parallel}{Y} \phi_\parallel \right). \tag{1.8}$$

Somiya et al. re-derived $\phi_\parallel$ and $\phi_\perp$ following a different route (Somiya, 2009)) and shew that the formulas in (1.3) are valid in the limit of vanishing Poisson ratios[6]. This suggests that eq. (1.8) could be a more consistent choice for use together with (1.3).

1.3 Minimum Noise Coatings

It is seen from (1.1) that coating Brownian noise can be reduced, in principle by i) reducing temperature T - note that this requires suitable modeling of the temperature dependence of the material loss angles entering in the formula for ϕ_c (see Chs. 4 and 8 in this book); ii) increasing the beam-width w (see the broad discussions in (O'Shaughnessy, 2006; Galdi et al., 2007), and Ch. 13 of Harry et al (2012)); iii) reducing the coating loss angle, by selecting and/or synthesizing low-loss materials (see Chs. 4 and 6 of this book), and/or optimizing the coating layers' thicknesses, under a prescribed reflectance (Agresti et al., 2006). More radical alternative mirror-design potentially capable of yielding substantial noise reduction, e.g., cavity-backed mirrors (Khalili, 2005) and coating free mirrors (Gössler et al., 2007) are still under investigation.
All these strategies (which are not mutually exclusive) have been explored during the last few years with varying degree of success, and are discussed in detail

[5] This limiting form appears in (Harry et al., 2002), eq. (23) with a misprint, an omitted $\perp$ suffix on the denominator of the second term in round brackets.

[6] Another derivation, where the coating materials (assumed isotropic) are characterized in terms of their complex shear and bulk moduli has been proposed by Y. Chen et al. (Hong et al., 2009).

in the companion Chapters of this Book.
Attention will be focused here on coating layers' thickness optimization, which has been experimentally demonstrated (Villar et al., 2010), and offers perhaps the best tradeoff to date between technological challenges/cost, and noise reduction.

1.3.1 Materials Downselection

Materials downselection has involved a considerable number of potential candidates, both for the substrate (SiO_2, Al_2O_3), and the coating (Al_2O_3, SiO_2, ZrO_2, Ta_2O_5, Nb_2O_5, TiO_2). The material downselection process eventually led to the present choice of fused Silica for the substrate (better than Sapphire in terms of thermoelastic noise). An important pre-requisite for coating materials are low optical losses. Among low-loss materials, the Silica-Tantala choice yields the best tradeoff between the desirable competing requirements of high-contrast and low mechanical losses, needed for low noise. See, e.g., (Crooks et al., 2006) for a discussion.
The possible use of glassy mixtures for the high-index coating material has also been investigated, with good results obtained from $Ta_2O_5 :: TiO_2$ co-sputtered formulas (Harry et al., 2007).

1.3.2 Blind Coating Thickness Optimization

Adopting a controlled ignorance attitude, genetic optimization[7] was used to find the structure of minimal noise coatings under a prescribed transmittance constraint, treating the total number of layers and the thicknesses of each layer as free independent parameters (Agresti et al., 2006). Genetic optimization was chosen in view of its known ability to handle non-convex optimization problems (Charbonneau, 2002).
The main result of this investigation was that optimized coatings display a neat tendency (as the number of optimization cycles is increased) toward configurations consisting of stacked identical low-high index doublets, except for the terminal (first/last) layers (Agresti et al., 2006). These doublets, are *not* quarter wavelength (QWL), as in the standard design. In the optimized coatings, the amount of Tantala (the noisier material) is reduced, while the number of doublets is slightly increased. On the basis of these findings, attention was focused on the analysis and optimization of coatings consisting of identical stacked-doublets.

1.3.3 Stacked Doublet Coatings

Stacked-doublet coatings (sketched in Figure 1) are (the simplest case of) truncated periodic multilayers using only two different dielectrics. Each elementary

[7] In particular, we used PIKAIA, a public domain genetic optimization engine. The PIKAIA SW is freely available at http://www.hao.ucar.edu/modeling/pikaia/pikaia.php.

doublet is described by the transmission matrix

$$\mathbf{D} = \mathbf{T}_L \cdot \mathbf{T}_H \tag{1.9}$$

where

$$\begin{cases} D_{11} = \cos\psi_L \cos\psi_H - (n_H/n_L)\sin\psi_L \sin\psi_H \\ D_{12} = \imath[(n_L)^{-1}\cos\psi_H \sin\psi_L + (n_H)^{-1}\cos\psi_L \sin\psi_H] \\ D_{21} = \imath[n_L \cos\psi_H \sin\psi_L + n_H \cos\psi_L \sin\psi_H] \\ D_{22} = \cos\psi_L \cos\psi_H - (n_L/n_H)\sin\psi_L \sin\psi_H \end{cases} . \tag{1.10}$$

The whole coating consisting of N_d doublets is accordingly described by the transmission matrix

$$\mathbf{T} = \mathbf{D}^{N_d} = \begin{bmatrix} D_{11} - \dfrac{\Psi_{N_d-2}(\Theta)}{\Psi_{N_d-1}(\Theta)} & D_{12} \\ D_{21} & D_{22} - \dfrac{\Psi_{N_d-2}(\Theta)}{\Psi_{N_d-1}(\Theta)} \end{bmatrix} \Psi_{N_d-1}(\Theta), \tag{1.11}$$

where

$$\Psi_N(\Theta) = \frac{\sin[(N+1)\Theta]}{\sin\Theta}, \ \Theta = \cos^{-1}\left[\frac{\mathrm{Tr}(\mathbf{D})}{2}\right], \tag{1.12}$$

and

$$\mathrm{Tr}(\mathbf{D}) = 2\cos\psi_1 \cos\psi_2 - \left(\frac{n_H}{n_L} + \frac{n_L}{n_H}\right)\sin\psi_1 \sin\psi_2 \tag{1.13}$$

is the trace of the doublet matrix.
The second equality in (1.11) follows from a well known property of unimodular matrices (see, e.g. Born and Wolf, 2005). For computational purposes it helps to recognize that[8]

$$\Psi_N(\Theta) = U_N\left[\frac{\mathrm{Tr}(\mathbf{D})}{2}\right] \tag{1.14}$$

U_N being the Chebychev polynomial of the second kind.

1.3.4 Stacked Doublet Coatings Loss Angle

Equation (1.8) for the coating loss angle can be easily rewritten in terms of the low/high index medium parameters. Letting

$$z_{L,H} = \frac{n_{L,H}}{\lambda_0} d_{L,H} \tag{1.15}$$

[8] It also helps noting that $\exp(\pm\imath\Theta)$ are the (Bloch) eigenvalues of $\mathbf{D}$, the corresponding eigenvectors being $\{D_{12}, \exp(\pm\imath\Theta) - D_{11}\}$. The reflection bands of the coating thus correspond to the forbidden bands of the infinite periodic structure.

the layer thicknesses in units of the local wavalength, we may write

$$\phi_c = \phi_0 \left(z_L + \gamma z_H \right), \tag{1.16}$$

where:

$$\phi_0 = \frac{N_d \lambda_0}{\sqrt{\pi} w} \frac{\phi_L}{n_L} \left(\frac{Y_L}{Y} + \frac{Y}{Y_L} \right), \tag{1.17}$$

and:

$$\gamma = \frac{\phi_H}{\phi_L} \frac{n_L}{n_H} \frac{\left(\frac{Y_H}{Y} + \frac{Y}{Y_H} \right)}{\left(\frac{Y_L}{Y} + \frac{Y}{Y_L} \right)}. \tag{1.18}$$

According to (1.16) the loss angle per unit thickness (scaled to the local wavelength) of the high-index material is γ times larger than that of the low-index material. For SiO_2/Ta_2O_5 doublets, $\gamma \approx 7$.

1.3.5 Minimal Noise Stacked Doublet Coatings

Figure 3 shows a number of constant-loss-angle contours (the straight lines), together with a number of iso-reflectance contours (the closed curves), in the (z_L, z_H) plane[9].
It is seen that the QWL design (the point $z_L = z_H = 0.25$) yields the largest reflectance at the corresponding fixed coating loss angle level. On the other hand, the design yielding the minimal coating loss angle for a prescribed transmittance corresponds to the point where the pertinent iso-reflectance contour is tangent (from above) to a constant ϕ_c contour. Such a point is the white marker in Figure 2. When the number of doublets becomes large (as implied by the large reflectances in order), the iso-reflectance contours squeeze unto the $z_L + z_H = 1/2$ line (the dashed line in Figure 2), and little error is made by taking the intersection between this latter and the iso-reflectance contour (the black marker in Figure 2) as the minimal noise design. Adopting this reasonable approximation[10], amounts to letting

$$z_H = \frac{1}{4} - \xi, \;\; z_L = \frac{1}{4} + \xi, \;\; \xi \in (0, 1/4) \tag{1.19}$$

which leaves only *two* free coating design parameters, namely, the number of doublets N_d and the quantity ξ in (1.19). This leads to the simple optimization algorithm below (Agresti et al., 2006; Villar et al., 2010):

```
1) start from the QWL design getting closest to the desired
```

[9]The former are obtained from (1.16) - (1.18); the latter from (1.55) - (1.57) and (1.11) - (1.13) .

[10]Kondratiev and Gorodetsky (Gorodetsky, 2010) derived a simple (implicit) formula yielding the lowest order correction in the dielectric contrast to the mentioned approximation. The added accuracy, hower, may be easily blurred by uncertainties and tolerances in the material parameters values.

```
      transmittance, for which ξ = 0 and N_d = N_d^(min);
2) add one doublet, and adjust ξ until the same transmittance
      is recovered;
3) calculate φ_c of the current coating configuration using
      eqs.  (1.16)-(1.19);
4) repeat steps 2)-3) until the minimum of φ_c is reached.
```

The results of this procedure are illustrated in Figure 3, for the special case[11] of a Silica/Tantala coating with a transmittance of $287ppm$ @ $1064nm$. Increasing the number of doublets (and in parallel increasing ξ, to keep the transmittance fixed) has a twofold effect: the fraction of higher-index (lossier) material (Tantala) is reduced, while the fraction of lower-index (less lossy) material (Silica) is increased. The coating loss angle ϕ_c in Figure 3 has a minimum for $N_d = 17$, corresponding to the tradeoff between these competing effects.
Note that the minimum in Figure 3 is rather *shallow*. This is nice, both in view of present uncertainties about the actual value of γ, and of possible variations due manufacturing tolerances.
As a matter of fact, the ϕ_c reduction featured by the optimal design with $N_d = 17$, compared to the QWL design, is changed by less than 2% when γ is allowed to vary between 5 and 10.
As already mentioned, the genetically optimized coatings differ from pure stacked-doublet configurations, because the terminal layers are different.
This suggests to modify the optimizationprocedure, by implementing a final step which consists in *tweaking* the terminal layers as follows (Villar et al., 2010):

```
1) tweak the top layer thickness so as to maximize the coat-
       ing reflectance;
2) tweak the bottom layer thickness so as to bring back the
       reflectance to the design value.
```

Numerical experiments indicate that tweaking successive layers beyond the terminal ones does *not* yield any appreciable further noise reduction. Also, we found no advantage in seeking for a minimum of the coating loss angle (at prescribed reflectance) using N_d, ξ, *and* the thicknesses of the top and bottom layer as free parameters, compared to the simplest sequential strategy where one first finds the optimal values of N_d and ξ for a pure stacked-doublet geometry, and subsequently tweaks the terminal layers, keeping N_d and ξ unchanged (Villar et al., 2010).

1.3.6 Optimized Prototypes

Optimized coating prototypes designed according to the above recipe were manufactured at the Laboratoire des Materiaux Avancees of CNRS (LMA, Lyon,

[11] These are the coating design figures for the Caltech Thermal Noise Interferometer mirrors (Black et al., 2004).

FR). Their noise PSD was measured using the Caltech Thermal Noise Interferometer ((Black et al., 2004), and Ch. 5 of Harry et al (2012)), and compared to that of a QWL coating having the same transmittance ($287ppm@1064nm$). See (Villar et al., 2010) for details.
A visual comparison between the (smoothed) noise PSD of the QWL and optimized coatings is shown in Figure 5, in a spectral region around 3 kHz, which is approximately at the center of the coating-dominated TNI noise spectrum. The separation between the noise spectra is apparent[12]. The loss angles can be estimated from the measured PSD, and are shown in Figure 5, toghether with the associated uncertainties, for a batch of runs[13]. The mean loss angles and their uncertainties are $\overline{\phi}_{opt} = (6.9 \pm 0.2) \times 10^{-6}$ and $\overline{\phi}_{QWL} = (8.4 \pm 0.3) \times 10^{-6}$, for the optimized and reference (QWL) coatings. The ratio of the means is $r = 0.82 \pm 0.04$, to be compared to the predicted value of 0.843 (for $\gamma = 7$), well within the uncertainty of the measured ratio (Villar et al., 2010). It is important to remind that the predicted loss-angle reduction ratio changes by less than 2% when γ is allowed to vary between 5 and 10.
It is worh mentioning at this point that simpler coating optimization strategies, based on the use of a *single* "compensating" layer, either within (Kimble et al., 2008) or on top (Gorodetsky, 2008) of the coating do not yield significant reductions in the coating loss angle (Kondratiev et al., 2011).

We conclude this Section by noting that the above analysis does not include the effects of the finite (transverse) size of the mirrors. Finite-size corrections for the mirror noise-components have been discussed in (Liu and Thorne, 2000) for the substrate noises, in (Somiya and Yamamoto, 2009) for the coating Brownian noise, and in (Braginsky and Vyatchanin, 2003) for the thermoelastic noise. These corrections do not affect or hinder the proposed coating optimization strategy to any sensible extent.

1.4 Dichroic Coatings

The latest AdLIGO design added the requirement of dual-wavelength operation for the cavity mirrors, both at the reference laser wavelength ($1064nm$) and its second harmonic ($532nm$), which will be used by the new locking system[14].
Traditional dichroic designs, using truncated bi-periodic structures (Lee et al., 1993; Lovering, 1996) is best suited to the case where comparable reflectances

[12]Note that there is no superposition between the confidence intervals of the fits (the dashed lines in Figure 4) since the error of the fits is much smaller than the standard deviation of the residuals.

[13]To be conservative, the standard deviation of *each* set of loss angles was used to set the uncertainties of the estimated means, rather than the usual standard deviation divided by the square root of the number of measurements made for each coating, which would be appropriate for Gaussian fluctuations (Villar et al., 2010).

[14]Further allowance for sufficient (loosely specified) reflectance at some (yet to be chosen) additional laser-friendly wavelength (e.g., $670, 946, 980, 1319$ or $1550nm$), used for Hartmann sensors and optical levers (see, e.g. Armandula et al., 2010) is requested.

on both bands are needed. In the LIGO case, the prescribed transmittances are quite different, the target values being 0.05 at $532nm$ and $5.5 \cdot 10^{-6}$ at $1064nm$.
A basic dichroic design consists in putting a stack of $(\lambda/4, \lambda/4)$ doublets on top of another stack of $(3\lambda/8, \lambda/8)$ doublets, λ being the reference wavelength in the material. At $532nm$ the top stack yields total transmission, the bottom stack is effectively QWL, and the number of its doublets can be chosen so as to yield the prescribed reflectance at that wavelength.
At the reference wavelength, $1064nm$, the topmost stack is QWL, and the number of its doublets can be chosen to supply the needed *extra* reflectance.
This design, originally proposed for AdLIGO, ignores material dispersion, which largely impairs its operation, and is by no means the minimal-noise design (Principe et al., 2008).
Blind genetic optimization can be used as a guide to identify the structure of minimal-noise coatings also for the dichroic case.
Similar to the single-wavelength case, genetically optimized minimal noise coatings subject to the mentioned (dichroic) transmittance constraints display a neat tendency (as the number of optimization cycles is increased) toward configurations consisting of identical low-high index doublets, except for the terminal layers (Pierro et al., 2009). The main difference with the single-wavelength case is that the phase thickness of each doublet is no longer π.
A minimal-noise dichroic stacked-doublet design can be accordingly sought by letting

$$z_L = \frac{1}{4} + \xi_L, \; z_H = \frac{1}{4} - \xi_H, \tag{1.20}$$

where now $\xi_L \neq \xi_H$, and using the total number of doublets N_d and the quantities ξ_L, ξ_H as the coating design parameters.
Figure 6 shows the coating loss-angle density plot computed by (1.16) in the (ξ_L, ξ_H) plane, together with the iso-transmittance/iso-reflectance contours corresponding to the prescribed transmittance/reflectance values at $1064nm$ and $532nm$, for a stacked doublet Silica/Tantala coating with $N_d = 18$. Clearly, two designs are possible fulfilling both transmittance/reflectance constraints, corresponding to the intersections between the two curves; the one corresponding to the white marker in Figure 6 yields the smaller loss angle.
Depending on N_d, the isoreflectance/isotransmittance curves corresponding to the target values may have two, one, or no common point (whenever there are two, one should select the one corresponding to the lower loss angle). For each N_d we accordingly get a $\{\xi_L, \xi_H\}$ pair and an associated loss-angle.
The optimization algorithm can be accordingly summarized as follows:

1) start from the minimum value of N_d for which the prescribed isotransmittance curves have a single common point;
2) add one doublet. Of the two isotransmittance curves intersections take the lower noise one;
3) repeat step 2) until the loss angle ϕ_c reaches a minimum.

Tweaking the terminal (first and last) layer is again in order, and can be used

in particular so as to satisfy the additional requirement of minimizing the total electric field at the mirror surface, while keeping the target transmittances unchanged. Prototype dichroic mirrors designed using the above recipe were manufactured by LMA, and successfully tested (Villar et al., 2009).

1.5 More Coating Noises

In this section we shall briefly overview additional coating noise terms, potentially affecting the operation of interferometric GW detectors. Within the limits of present day technologies, Brownian noise is by far the dominant coating noise term, but progresses in optical materials and coating design may change the situation in a few years.

1.5.1 Thermo Optic Noise

Fluctuations in the coating temperature may have a twofold origin: thermodynamic and photothermal. The latter stem from fluctuations in the laser intensity, resulting into fluctuations of the power dissipated in the coating. The power spectral density of both kinds of temperature fluctuations have been computed in (Braginsky et al., 2000) and (Braginsky et al., 1999), and are, respectively

$$S_{\Delta T}^{(\Theta)}(f) = \frac{k_B T^2}{\pi^{3/2} r_0^2 \sqrt{f \chi_S C_S \rho_S}}, \tag{1.21}$$

$$S_{\Delta T}^{(\Phi)}(f) = \frac{P_{abs} E_\lambda}{4\pi^3 r_0^4 \chi_S \rho_S C_S f}, \tag{1.22}$$

where, as usual, k_B is Boltzmann's constant, T the temperature, r_0 the beam radius, χ_S, ρ_S and C_S are the thermal conductivity, density, and heat capacity of the substrate, P_{abs} is the power dissipated in the coating due to optical losses, E_λ the beam photon energy, and f the frequency.
The underlying mechanisms being independent, the thermodynamic and photothermal fluctuations are uncorrelated, and their power spectral densities add incoherently to form the power spectral density of the coating temperature fluctuations

$$S_{\Delta T}(f) = S_{\Delta T}^{(\Theta)}(f) + S_{\Delta T}^{(\Phi)}(f). \tag{1.23}$$

Temperature fluctuations in the end mirrors imply fluctuations in the cavity phase length, via thermal expansion (thermoelastic noise), and temperature dependence of the refraction index of the coating materials (thermorefractive effect).
It is expedient to define the quantities[15]. α_{eff}, β_{eff}

$$\frac{\Delta z^{(TE)}}{d_{tot}} = \alpha_{eff} \Delta T \tag{1.24}$$

[15]In general, eqs. (1.24), (1.25) should be understood as being written in the spectral domain, α_{eff} and β_{eff} representing frequency-dependent complex transfer functions.

$$\frac{\Delta z^{(TR)}}{\lambda_0} = -\beta_{eff}\Delta T \tag{1.25}$$

relating, respectively, the (actual or equivalent) displacement of the mirror front face to a temperature change ΔT, with $d_{tot} = N_d(d_L+d_H)$ the total thickness of the coating, and λ_0 the beam wavelength .
The superscripts TE and TR in (1.24), (1.25) identify the thermoelastic and thermorefractive displacement components, and the quantities α_{eff} and β_{eff} are the coating thermoelastic and thermorefractive coefficients.
The power spectral densities of the thermoelastic and/or thermorefractive displacements can be simply obtained thereafter, by Wiener-Khinchin theorem ,

$$S_z(f) = \mathcal{F}_{\tau\to f}\langle\Delta z(t)\Delta z(t+\tau)\rangle_t = |H_{\Delta z}|^2 S_{\Delta T}(f) \tag{1.26}$$

where $\mathcal{F}$ is the Fourier transform operator, the angle-brackets denote (integral) time-averaging, and $H_{\Delta z}$ denotes the spectral transfer function connecting Δz to ΔT.

1.5.2 Thermoelastic Coefficient

A formula for α_{eff} was first derived in (Braginsky and Vyatchanin, 2003) (the post-publication version of this paper (v5) available in ArXiv contains important fixes and additions) and indipendently obtained in (Fejer et al., 2004). Merging those results, it is possible to write

$$\alpha_{eff} = \alpha_L\frac{d_L}{d_L+d_H} + \alpha_H\frac{d_H}{d_L+d_H} \tag{1.27}$$

where

$$\alpha_{L,H} = 2(1+\sigma_S)\left\{\frac{\alpha_{L,H}}{2(1-\sigma_{L,H})}\left[\frac{1+\sigma_{L,H}}{1+\sigma_S}+(1-2\sigma_S)\frac{Y_{L,H}}{Y_S}\right]-\alpha_S\frac{C_{L,H}}{C_S}\right\}\cdot$$
$$\cdot\left(\frac{g(\omega)}{g(0)}\right)^{1/2}\Xi_{fsm}^{1/2} \tag{1.28}$$

all symbols having the usual meaning. The frequency dependent factor $g(\omega)$ was introduced in (Fejer et al., 2004), and is

$$g(\omega) = Im\left\{-\frac{\sinh[(\imath\omega\tau_f)^{1/2}]}{(\imath\omega\tau_f)^{1/2}\left[\cosh[(\imath\omega\tau_f)^{1/2}]+R\sinh[(\imath\omega\tau_f)^{1/2}]\right]}\right\} \tag{1.29}$$

with

$$\tau_f = \frac{(d_L+d_H)C_f}{\chi_f},\ R = \left(\frac{\chi_f C_f}{\chi_S C_S}\right)^{1/2}, \tag{1.30}$$

and

$$\chi_f = (d_L+d_H)\left(\frac{d_L}{\chi_L}+\frac{d_H}{\chi_H}\right)^{-1} = \langle\chi_i\rangle_R,$$
$$C_f = \frac{d_L C_L + d_H C_H}{d_L+d_H} = \langle C_i\rangle_V \tag{1.31}$$

The factor $\Xi_{fsm}(\omega)$, accounting for the finite size of the mirror, has been first derived in (Braginsky and Vyatchanin, 2003), and can be written

$$\Xi_{fsm} = \bar{r}_0 \frac{(\Pi/2)^{1/2}}{\Lambda(1+\nu_S)}. \tag{1.32}$$

where $\bar{r}_0 = r_0/R_m$, R_m being the mirror radius. The quantities Λ and Π in (1.32) are given by (Braginsky and Vyatchanin, 2003)

$$\Lambda = \sum_{i=L,H} \frac{d_i}{d_L+d_H}\left[-\frac{C_i}{C_S} + \frac{\alpha_i(1+\nu_i)}{2\alpha_S(1-\nu_i)(1+\nu_S)} + \frac{Y_i(1-2\nu_S)}{Y_S(1-\nu_i)}\right] \tag{1.33}$$

and

$$\Pi = [U + VS_1]^2 + S_2 \tag{1.34}$$

where[16]

$$U = \sum_{i=L,H} \frac{d_i}{d_L+d_H}\left[\frac{\alpha_S}{\alpha_i}\left(\frac{1+\nu_i}{1-\nu_i} - \frac{2\nu_S Y_i}{E_S(1-\nu_i)}\right) - \frac{C_i}{C_S}\right] \tag{1.35}$$

$$V = \sum_{i=L,H} \frac{d_i}{d_L+d_H}\left(\frac{C_i}{C_S} - \frac{\alpha_i Y_i(1-\nu_s)}{\alpha_S Y_s(1-\nu_i)}\right) \tag{1.36}$$

$$S_1 = 12\bar{h}^{-2}\sum_{m=0}^{\infty} \frac{\exp(-\zeta_m^{(1)}\bar{r}_0^2/4)}{(\zeta_m^{(1)})^2 J_0(\zeta_m^{(1)})} \tag{1.37}$$

$$S_2 = \sum_{m=1}^{\infty} \Lambda_m^2 \frac{exp[-(\zeta_m^{(1)}\bar{r}_0)^2/2]}{J_0^2(\zeta_m^{(1)})} \tag{1.38}$$

In (1.37), (1.38) $\zeta_m^{(1)}$ the m-th zero of Bessel function J_1, $\bar{h} = H_m/R_m$, H_m being the mirror height, and

$$\Lambda_m = A + B\Upsilon_m \tag{1.39}$$

with

$$A = \sum_{i=L,H} \frac{d_i}{d_L+d_H}\left[\frac{\alpha_i(1+\nu_i)}{\alpha_S(1-\nu_i)} - \frac{1+\nu_S}{1-\nu_i}\right] \tag{1.40}$$

$$B = \sum_{i=L,H} \frac{d_i}{d_L+d_H}\left[\frac{\alpha_i Y_i(1-2\nu_S)}{\alpha_S Y_S(1-\nu_i)} + \frac{1}{1-\nu_i} - 2\frac{C_i}{C_S}\right] \tag{1.41}$$

and

$$\Upsilon_m = \frac{(1+\nu_S)[1-\exp(-2\zeta_m^{(1)}\bar{r}_0)]}{[1-\exp(-2\zeta_m^{(1)}\bar{r}_0)] - 4(\zeta_m^{(1)}\bar{h})^2\exp(-2\zeta_m^{(1)}\bar{r}_0)}. \tag{1.42}$$

[16] The infinite sums in $S_{1,2}$ converge rapidly: 30 terms are sufficient to achieve 16 figures precision.

1.5.3 Thermorefractive Coefficient

A simple closed form expression for the thermorefractive coefficient β_{eff} valid for QWL coatings was given (Braginsky et al., 2000), based on a self consistency argument valid for high reflection stacked doublet coatings, for which the addition of a further doublet does not change appreciably the coating input impedance:

$$\beta_{eff} = \frac{n_H^2 \beta_L + n_L^2 \beta_H}{4(n_H^2 - n_L^2)} \tag{1.43}$$

the same formula was obtained in (Principe et al., 2007) using a different route (complete induction), disproving an alternative formula in [Braginsky et al., 2003b].
Equation (1.43) was generalized in (Principe et al., 2007) to general stacked-doublet coatings. The resulting expression is

$$\beta_{eff} = \frac{1}{2\pi\imath} \frac{\dot{\overline{Y_c}}}{1 - \overline{Y_c}^2} \tag{1.44}$$

where $\overline{Y_c}$ is the coating input admittance (normalized to the vaccum one), and the dot denotes derivative with respect to temperature. Both $\dot{\overline{Y_c}}$ and $\overline{Y_c}$ can be written in terms of the doublet matrix elements in (1.10) as follows (Principe et al., 2007)

$$\overline{Y_c} = -\frac{(D_{11} - D_{22}) + \sqrt{(D_{11} - D_{22})^2 - 4D_{12}D_{21}}}{2D_{12}}. \tag{1.45}$$

$$\dot{\overline{Y_c}} = \frac{\dot{D}_{21} + \overline{Y_c}(\dot{D}_{22} - \dot{D}_{11}) - \overline{Y_c}^2 \dot{D}_{12}}{D_{11} - D_{22} + 2\overline{Y_c}\dot{D}_{12}} \tag{1.46}$$

Both the thermoelastic and thermorefractive coefficients can be minimized by reducing the relative amount of high index (more noisy) material in the coating. This is similar to the Brownian case, and suggests that even if thermoelastic and/or thermorefractive noise were comparable to Brownian noise, one may still use the optimization strategy discussed in Section 1.3.5 to minimize the *total* coating noise.

1.5.4 Thermooptic Noise Cancellation

It is expected on physical grounds (coating thickness and field build-up time are much smaller than the corresponding decorrelation scales of the temperature fluctuations) that thermoelastic and thermorefractive displacements should be added coherently[17], so that

$$|H_{\Delta z}|^2 = |d_{tot}\alpha_{eff} - \lambda_0 \beta_{eff}|^2 . \tag{1.47}$$

[17] In the extreme opposite case where thermoelastic and thermorefractive displacements were totally incorrelated,

$$|H_{\Delta z}|^2 = \left|d_{tot}\alpha_{eff}\right|^2 + \left|\lambda_0 \beta_{eff}\right|^2.$$

in (1.26). As shown in (Evans et al., 2008), adding coherently the thermoelastic and thermorefractive terms with the right relative signs[18] entails partial cancellation between the two terms. Experimental checks of this cancellation using the TNI are underway (Ogin, 2009).
Exact cancellation may occur (assuming positive values for the α_i and the β_i) for some specific (non-QWL) coating configuration, in a frequency dependent way (Castaldi et al., 2008), due to the ω-dependent factor in the thermoelastic coefficient (1.28).
Luckily, coating designs optimized for minimal Brownian noise are also *nearly* optimized, throughout the spectral band of interest for GW observations, when thermooptic noise is included (Castaldi et al., 2008).

1.6 Optical Properties of Coatings

In this section we summarize the basic formulas on which optical coating characterization is based. The interested Reader will find a compact ab-initio derivation of these results in Appendix-A of Chapter 12 in Harry et al (2012).
Coatings are modeled as stacks of planar layers terminated on both sides by homogeneous half spaces; the relevant geometry and notation is sketched in Figure 1. Layers are identified by an index $i=1,2,\ldots,N_L$. It is understood that $i=0$ and $i=N_L+1$ correspond to the left halfspace and the substrate, respectively.
It is convenient to introduce a local coordinate system (x, y, z_i) for each layer, so that the internal layers $i = 1, 2, \ldots, N_L$ correspond to $-d_i \leq z_i \leq 0$, the left halfspace is defined by $-\infty < z_0 \leq 0$, and the substrate by $0 \leq z_{N_L+1} < \infty$.
Plane wave incidence from the leftmost halfspace is assumed. An $\exp(\imath\omega t)$ time dependence of the field is understood and omitted.

1.6.1 Singlet Matrix

Consider normal incidence first, where the field in each layer is a linearly polarized plane wave whose wave vector is normal to the (planar, parallel) interfaces. The properties of a *singlet*, i.e., a planar homogeneous layer with finite thickness d_i and (complex) refractive index $n^{(i)}$ are described by the transmission matrix

$$\mathbf{T}_i = \begin{bmatrix} \cos\psi_i & \imath(n^{(i)})^{-1}\sin\psi_i \\ \imath n^{(i)}\sin\psi_i & \cos\psi_i \end{bmatrix} \tag{1.48}$$

where

$$\psi_i = \frac{2\pi}{\lambda_0} n^{(i)} d_i, \tag{1.49}$$

is the phase-thickness of the layer, λ_0 being the light wavelength in vacuum. The matrix (1.48) relates the nonzero transverse components of the electric and

[18] In Castaldi et al. (2007) the coherent superposition was computed with a wrong relative sign.

magnetic field at the singlet terminal planes as follows

$$\begin{bmatrix} E^{(i)} \\ Z_0 H^{(i)} \end{bmatrix}_{z_i=-d_i} = \mathbf{T}_i \cdot \begin{bmatrix} E^{(i)} \\ Z_0 H^{(i)} \end{bmatrix}_{z_i=0}. \tag{1.50}$$

A vacuum characteristic impedance $Z_0 = (\mu_0/\epsilon_0)^{1/2}$ factor is inserted in front of the magnetic fields in (1.50) so as to make the transmission matrix dimensionless. The singlet matrix (1.48) is unimodular, i.e., det $\mathbf{T}_i = 1$.
Maxwell equations require the transverse field components to be continuous across the layer interfaces. Hence

$$\begin{bmatrix} E_t^{(i)} \\ Z_0 H_t^{(i)} \end{bmatrix}_{z_i=-d_i} = \begin{bmatrix} E_t^{(i-1)} \\ Z_0 H_t^{(i-1)} \end{bmatrix}_{z_{i-1}=0}. \tag{1.51}$$

Accordingly,

$$\begin{bmatrix} E^{(1)} \\ Z_0 H^{(1)} \end{bmatrix}_{z_1=-d_1} = \mathbf{T} \cdot \begin{bmatrix} E^{(N_L)} \\ Z_0 H^{(N_L)} \end{bmatrix}_{z_{N_L}=0}, \tag{1.52}$$

where

$$\mathbf{T} = \mathbf{T}_1 \cdot \mathbf{T}_2 \cdot \ldots \cdot \mathbf{T}_{N_L} \tag{1.53}$$

is the whole multi-layer transmission matrix.
In the substrate only a forward propagating plane wave exists, so that

$$E^{(N_L+1)} = Z^{(N_L+1)} H^{(N_L+1)} = (n^{(N_L+1)})^{-1} Z_0 H^{(N_L+1)}, \tag{1.54}$$

$Z^{(N_L+1)} =: Z_S$ and $n^{(N_L+1)} =: n_S$ being the substrate characteristic impedance and refraction index, respectively. From (1.52) and (1.54) it is possible to compute the input impedance Z_c of the whole substrate-terminated coating, and its effective refractive index n_c

$$\frac{E^{(1)}}{Z_0 H^{(1)}} =: \frac{Z_c}{Z_0} = (n_c)^{-1} = \frac{T_{11} + n_S T_{12}}{T_{21} + n_S T_{22}}. \tag{1.55}$$

The (complex) coating reflection coefficient is thus

$$\Gamma_c = \frac{n^{(0)} - n_c}{n^{(0)} + n_c}, \tag{1.56}$$

and the power transmittance is

$$\tau_p = 1 - |\Gamma_c|^2. \tag{1.57}$$

Alternatively[19], the coating reflection coefficient can be retrieved from the Airy-Schur formula:

$$\Gamma_{i-1} = \frac{\gamma_{i-1,i} + \Gamma_i \exp(-2\imath\psi_i)}{1 + \gamma_{i-1,i}\, \Gamma_i \exp(-2\imath\psi_i)}, \tag{1.58}$$

[19]Equations (1.53)-(1.56) and (1.58) have different error propagation properties. When dealing with truncated-periodic multilayers, using (1.53)-(1.56) yields better accuracy.

where Γ_i is the ratio between the (complex) forward and backward wave amplitudes at $z_i = 0$, and

$$\gamma_{i-1,i} = \frac{n^{(i-1)} - n^{(i)}}{n^{(i-1)} + n^{(i)}} \tag{1.59}$$

is the reflection coefficient fro a wave incident at the interface from a half space with $n = n^{(i-1)}$ to a half-space with $n = n^{(i)}$.
The coating reflection coefficient is obtained by iterating (1.58) from $i = N_L$, where $\Gamma_{N_L} = \gamma_{N_L,N_L+1}$ down to $i = 1$. where $\Gamma_1 = \Gamma_c$.

1.6.2 Oblique Incidence

The normal-incidence results in the previous section are readily extended to the case of a general elliptically polarized obliquely incident plane wave. Such a wave can be always decomposed into the superposition of linearly polarized transverse-electric (TE) and transverse-magnetic (TM) plane waves, where, respectively, the electric field and the magnetic field is orthogonal to the incidence plane, defined by the normal to the interface(s) and the incident field wave-vector (the xz plane in Figure 1).
Equations (1.48)-(1.50) are still valid, provided the transverse fields components in (1.50) are identified as follows:

$$(E_t, H_t) = \begin{cases} (E_y, -H_x), \text{ for TE incidence} \\ (E_x, H_y), \text{ for TM incidence} \end{cases}, \tag{1.60}$$

once the following formal substitution are made,

$$n^{(i)} \longrightarrow n_T^{(i)} = \begin{cases} n^{(i)} \cos\theta_i, \text{ for TE incidence} \\ n^{(i)}/\cos\theta_i, \text{ for TM incidence} \end{cases}, \tag{1.61}$$

and the phase thickness formula (1.49) is replaced by

$$\psi_i = \frac{2\pi}{\lambda_0} n^{(i)} d_i \cos\theta_i, \tag{1.62}$$

The quantities n_T and $Z_T = Z_0/n_T$ are referred to as the *transverse* refraction index and characteristic impedance, respectively.
The angles θ_i ($i = 1, 2, \ldots, N_s$) and θ_{sub} needed to compute the transverse indexes (1.61) and the phase thickness (1.62) are obtained from the incidence angle θ_0 by repeated application of Snell's law,

$$n^{(0)} \sin\theta_0 = n^{(1)} \sin\theta_1 = \ldots = n^{(N_L)} \sin\theta_{N_L} = n^{(N_L+1)} \sin\theta_{N_L+1}. \tag{1.63}$$

For orthogonal incidence $\theta_0 = 0$, the TE and TM cases are physically equivalent (except for an irrelevant rotation around the z-axis), all θ_i are zero, and $n_T^{(i)} = n^{(i)}$.

1.6.3 Optical Losses

Lossy materials are characterized by complex refraction indexes

$$\tilde{n}^{(i)} = n^{(i)} - \imath\kappa^{(i)}. \tag{1.64}$$

$\kappa > 0$ being known as the extinction coefficient. All equations (1.48)-(1.63) remain valid, after the analytic continuation $n \to \tilde{n}$.
Snell's law (1.63) yields now *complex* values for the $\sin\theta_i$, and the root sign in

$$\cos\theta_i = (1 - \sin\theta_i^2) = \left[1 - \left(\frac{\tilde{n}^{(i-1)}}{\tilde{n}^{(i)}}\sin\theta_{i-1}\right)^2\right]^{1/2}. \tag{1.65}$$

should be chosen so that

$$Im(\cos\theta_i) \leq 0. \tag{1.66}$$

The average power (per unit area) absorbed in all coating layers with $i \geq m$, including the substrate, is

$$\mathcal{P}_{[i\geq m]} = \frac{1}{2}Re\left(\vec{E_t}^{(m-1)} \times \vec{H_t}^{(m-1)*} \cdot \hat{z}\right)_{z_{m-1}=0} \tag{1.67}$$

where the asterisk denotes complex conjugation. The power absorbed in layer $i = m$ is thus

$$\mathcal{P}_m = \mathcal{P}_{[i\geq m]} - \mathcal{P}_{[i\geq m+1]}. \tag{1.68}$$

For $m = 1$

$$E_t^{(0)} = E_t^{(0),+}(1 + \Gamma_c),\ Z_0 H_t^{(0)} = \tilde{n}_T^{(0)} E_t^{(0),+}(1 - \Gamma_c), \tag{1.69}$$

at $z_0 = 0$, and hence (assuming $\kappa^{(0)} = 0$)

$$\mathcal{P}_{[i\geq 1]} = n_T^{(0)}\mathcal{P}^{(0),+}(1 - |\Gamma_c|^2), \tag{1.70}$$

where $E_t^{(0),+}$ is the known (complex) amplitude of the incident plane wave at the coating interface, and

$$\mathcal{P}^{(0),+} = \frac{1}{2Z_0}\left|E_t^{(0),+}\right|^2 \tag{1.71}$$

is the related (known) power density per unit area in vacuum.
Using the inverse of (1.50), viz.

$$\begin{bmatrix} Et^{(m)} \\ Z_0 H_t^{(m)} \end{bmatrix}_{z_m=0} = \mathbf{T}_m^{-1} \cdot \begin{bmatrix} E_t^{(m-1)} \\ Z_0 H_t^{(m-1)} \end{bmatrix}_{z_{m-1}=0}, \tag{1.72}$$

equations (1.67) and (1.68) allow to compute recursively, starting from $m = 1$, the power (per unit cross section) dissipated in each layer of the coating.

1.7 Material Parameters

Noise calculations, and coating design optimization are obviously dependent on the availability of reliable values for the pertinent material parameters.
In this section we shall limit our discussion to the coating materials presently in use for GW interferometers (SiO_2, Ta_2O_5, TiO_2).
The coating loss angle of SiO_2 thin films has been measured to high accuracy (Penn et al., 2010), yielding $\phi = (5 \pm 2) \cdot 10^{-5}$. The loss angle for Ta_2O_5 and $Ta_2O_5 :: TiO_2$ has been recently estimated (A. Villar et al., 2010b) from TNI-based direct measurements of the loss angle in a number of coating prototypes using different geometries and materials. The estimated values are $(4.7 \pm 0.5) \cdot 10^{-4}$ for Ta_2O_5 and $(3.7 \pm 0.3) \cdot 10^{-4}$ for $Ta_2O_5 :: TiO_2$ (LMA "formula V"). These values differ somewhat from those obtained by measuring the damping constant of cantilever or membrane shaped specimens, for reasons yet to be understood. Note that the values presently in use for all other relevant parameters (elastic modulus Y, poisson ratio σ, etc.) are fiducially assumed as being equal to their bulk counterparts.
Thermoelastic and thermorefractive coefficients are presently known with much less accuracy. For Ta_2O_5, values of α ranging from $-(4.43 \pm 0.05) \cdot 10^{-4}\ K^{-1}$ (Naci Inci and Yoshino, 2000) to $(5. \pm 2.) \cdot 10^{-6}\ K^{-1}$ (Braginsky and Vyatchanin, 2003) and values for β ranging from $(2.3 \pm 2.) \cdot 10^{-6}\ K^{-1}$ (Braginsky and Vyatchanin, 2003) to $(1.2 \pm 2.) \cdot 10^{-4}\ K^{-1}$ (Naci Inci, 2004) have been reported.
Luckily, as already mentioned, uncertainties in the thermo/optic coefficients have almost no impact on total coating noise, and coating design optimization. Reliable numbers are expected from ongoing direct measurements on actual coating prototypes (Gretarsson, 2009). These measurements face the basic difficulty of disentangling the thermoelastic and thermorefractive contributions. Measurements taken at different wavelengths could do the job, provided a suitable model for the wavelength dependence of the α, β parameters is assumed.
Concerning $Ta_2O_5 :: TiO_2$ mixtures, it is worth noting that sputtered TiO_2 films are known to exhibit a *negative* thermorefractive coefficient β (Xie et al., 2008). Co-sputtered mixtures involving Titania may thus be expected to exhibit positive or negative β, depending on Titania concentration. This has been observed, eg., in Silica::Titania mixtures (Hirota al., 2005).

Bibliography

Agresti J. et al. 2006, "Optimized Multilayer Dielectric Mirror Coatings for Gravitational Wave Interferometers," *Proc. SPIE*, **6286**, also available as LIGO Document P060027 (2006).

Armandula H., et al. 2010, "Core Optics Components Final Design," LIGO Technical Document T100038.

Black E.D. et al. 2004, "Direct Observation of Broadband Coating Thermal Noise in a Suspended Interferometer," *Physics Lett.*, **A328**, 1.

Born M. and Wolf E. 2005, *Optics*, Pergamon Press.

Braginsky V.B., Gorodetsky M.L. and Vyatchanin S.P. 1999, "Thermodynamical Fluctuation and Photothermal Shot Noise in GW Antennase," *Physics Lett.*, **264**, 1.

Braginsky V.B., Gorodetsky M.L. and Vyatchanin S.P. 2000, "Thermorefractive Noise in GW Antennae," *Physics Lett.*, **A271**, 303.

Braginsky V.B., Vyatchanin S.P. 2003, "Thermodynamical Fluctuations in Optical Mirror Coatings," *Physics Lett.*, **A312**, 244; see also ArXiv:cond-mat/0302617 v5, for important post-publication additions.

Castaldi G. et al. 2007, "Coating Design Optimization for Advanced Interferometers: Minimization of Total Noise Budget," LIGO Document G070309.

Castaldi G. et al. 2008, "Status of Coating Work at Sannio," LIGO Document G080487.

Chao S., Wang W.-H. and Lee, C.C. 2001, "Low Loss Dielectric Mirror with Ion Beam Sputtered $TiO_2 - SIO_2$ Mixed Film," *Appl. Opt.*, **40**, 2177.

Charbonneau P. 2002, "An Introduction to Genetic Algorithms for Numerical Optimization," NCAR Technical Note TN-450+IA.

Crooks D.R.M. et al. 2002, "Excess Mechanical Loss Asasociated with Dielectric Mirror Coatings on Test Masses in Interferometric GW Detectors," *Class. Quantum Grav.*, **19**, 883.

Crooks D.R.M. et al. 2006, "Experimental Measurements of Mechanical Dissipation Associated with Dielectric Coetings Formed Using SiO2, Ta2O5 and Al2O3," *Class. Quantum Grav.*, **23**, 4953.

Evans M. et al. 2008, "Thermo Optic Noise in Coated Mirrors for High Precision Optical Measurements," *Phys. Rev.*, **D78**, 102003.

Fejer M.M. et al. 2004, "Thermoelastic Dissipation in Inhomogeneous Media: Loss Measurements and Displacement Noise in Coated Test Masses for Interferometric GQW Detectors," *Phys. Rev.*, **D70**, 082003.

Pierro V. et al. 2007, "Perspectives on Beam-Shaping Optimization for Thermal-Noise Reduction in Advanced Gravitational-Wave Interferometric Detectors: Bounds, Profiles, and Critical Parameters," *Phys. Rev.*, **D76**, 122003.

Ghosh G. et al. 1994, "Temperature Dependent Sellmeier Coefficients and Chromatic Dispersions for Some Optical Fiber Glasses," *J. Lightwave Tech.*, **12**, 1338.

Gorodetsky M. 2008, "Thermal Noises and Noise Compensation in High Reflection Multilayer Coatings," *Physics Lett.*, **A372**, 6813.

Gorodetsky M. 2010, personal communication.

Gössler S. et al. 2007, "Coating Free Mirrors For High Precision Interferometric Experiments," LIGO Document P070069.

Gretarsson A. 2009, "Problems measuring the thermo-optic parameters for tantala/silica coatings," LIGO Document G0900224.

Gurkovsky A. and Vyatchanin S. 2010, "The Thermal Noise in Multilayer Coatings," *Physics Lett.*, **A374**, 3267.

Hong T., Yang H. and Chen Y. 2009, "Anatomy of Brownian Thermal Noise in the Coated Mirrors," LIGO Document G0900906.

G. Harry et al., Eds., *Optical Coatings and Thermal Noise in Precision Measurements,* Cambridge University Press, 2012.

Harry G.M. et al. 2002, "Thermal Noise in Interferometric GW Detectors due to Optical Coatings," *Class. Quantum Grav.*, **19**, 897.

Harry G.M. et al. 2004, "Incorporating Coating Anisotropy into Coating Thermal Noise," LIGO Document T040029.

Harry G.M. et al. 2006, "Thermal Noise from Optical Coatings in GW Detectors," *Applied Optics*, **45**, 1569.

Harry G.M. et al. 2007, "Titania Doped Tantala/Silica Coatings for Gravitational Wave Detection," *Class. Quantum Grav.*, **24**, 405.

Hirota H. et al. 2005, "Temperature Coefficients of Refractive Indices of TiO_2SiO_2 Films," *Jap. J. Appl. Phys.*, 44, 1009.

Khalili F.Y. 2005, "Reducing the Mirrors Coating Noise in Laser GW Antennae by Means of Double Mirrors," *Phys. Rev.*, **D334**, 67.

Kimble H.J., Lev N.L. and Ye J. 2008, "Optical Interferometers with Reduced Sensitivity to Thermal Noise," *Phys. Rev. Lett.*, **101**, 260602.

Kondratiev N.M., Gurkovsky A.G. and Gorodetsky M.L. 2011, "Effect of Interference on Thermal Noise and Coating Optimization in Dielectric Mirrors," LIGO Document P1000145.

Kubo R. 1966, "The Fluctuatio-Dissipation Theorem," *Rep. Prog. Phys.*, **29**, 255.

Lakes S.R. 2009, *Viscoelastic Materials*, Cambridge University Press.

Lee C.C. and Tang C.-J. 2006, "$TiO_2 - Ta_2O_5$ Thin Films Deposited by RF Ion Beam Sputtering," *Appl. Opt*, **45**, 9125.

Lee C.P., Tsai C.M. and Tang J.S. 1993, "Dual Wavelength Bragg Reflectors Using GaAs/AlAs Multilayers," *Electronics Lett.*, **29**, 1980.

Levin Yu. 1998, "Internal Thermal Noise in the LIGO Test Masses: a Direct Approach," *Phys. Rev.*, **D57**, 659.

Liu Y.T. and Thorne K.S. 2000, "Thermoelastic Noise and Homogeneous Thermal Noise in Finite Sized Gravitational Wave Test Masses," *Phys. Rev.*, **D62**, 122002.

Lovering D.J. et al. 1996, "Optimisation of Dual-Wavelength Bragg Mirrors," *Electronics Lett.*, **32**, 1782.

Naci Inci M. and Yoshino T. 2000, "A Fiber Optic Wavelength Modulation Sensor Based on Tantalum Pentoxide Coatings for Absolute Temperature Measurement," *Opt. Rev.*, **7**, 205.

Naci Inci M. 2004, "Simultaneous Measurement of the Thermal Optical and Linear Thermal Expansion Coefficients of a Thin Film Etalon from the Reflection Spectra of a Superluminescent Diode," *J. Appl. Phys.*, **D37**, 3151.

Netterfeld R.P. and Gross M. 2007, "Investigation of Ion Beam Sputtered Silica-Titania Mixtures for Use in GW Detectors," in *Proc. Optical Interference Coatings*, OSA Technical Digest (CD), paper ThD2.

Ogin G. 2009, "Thermo-Optic Coating Response Measurements," LIGO Document G0900265.

O'Shaughnessy R. 2006, "A Note on Coating Thermal Noise for Arbitrary-Shaped Beams ," *Class. Quantum Grav.*, **23**, 7627.

Penn S.D. et al. 2003, "Mechanical Loss in Tantala/Silica Dielectric Mirror Coatings," *Class. Quantum Grav.*, **20**, 2917.

Penn S.D. et al. 2010, "Recent Measurements of Coating and Substrate Mechanical Loss for aLIGO," LIGO Document G1000932.

Pinto I.M. et al. 2009, "Coating Optimization Update." LIGO Document G0900205.

Pinto I.M. et al. 2010, Mixture Theory Approach to Coating Materials Optimization," LIGO Document G1000537.

Principe M., Pinto I.M. and Galdi V. 2007, "A General Formula for the Thermorefractive Noise Coefficient of Stacked-Doublet Mirror Coatings," LIGO Technical Document T071599.

Principe M. et al. 2008, "Minimum Brownian Noise Dichroic Dielectric Mirror Coatings for AdLIGO," LIGO Technical Document T080337.

Rao S. 2003, "Mirror Thermal Noise in Interferometric GW Detectors," PhD Thesis, Caltech.

Scott W.W. and MacCrone R.K. 1968, "Apparatus for Mechanical Loss Measurements at Audio Frequencies and Low Temperatures," *Rev. Sci Instr.*, **39**, 821.

Somiya K. 2009, "Discussion about Losses in the Perpendicular and Parallel Directions," LIGO Technical Document T0900033.

Somiya K. and Yamamoto K. 2009, "Coating Thermal Noise of a Finite Size Cylindrical Mirror," *Phys. Rev.*, **D79**, 102004 .

Stenzel O. et al. 2011, "Mixed-Oxide Coatings for Optixs," *Appl. Optics*, **50**, C69.

Villar A.E. et al. 2009, "Measurement of Brownian Noise in Titania-Doped Tantala Coatings," LIGO Document G0900887.

Villar A.E. et al. 2010, "Measurement of Thermal Noise in Multilayer Coatings with Optimized Layer Thicknesses," *Phys. Rev.*, **D81**, 122001.

Villar A.E. et al. 2010b, "Loss Angles from the Direct Measurement of Brownian Noise in Coatings," LIGO Document G1000937.

Wang W.-H. and Chao S. 1998, "Annealing Effect on Ion-Beam Sputtered Titanium Dioxide Films," *Opt. Lett.*, **23**, 1417.

Xie H. et al. 2008, "Temperature Dependent Properties of Titanium Oxide Thin Films by Spectroscopic Ellipsometry," *SimTech Reports*, **9**, 29.

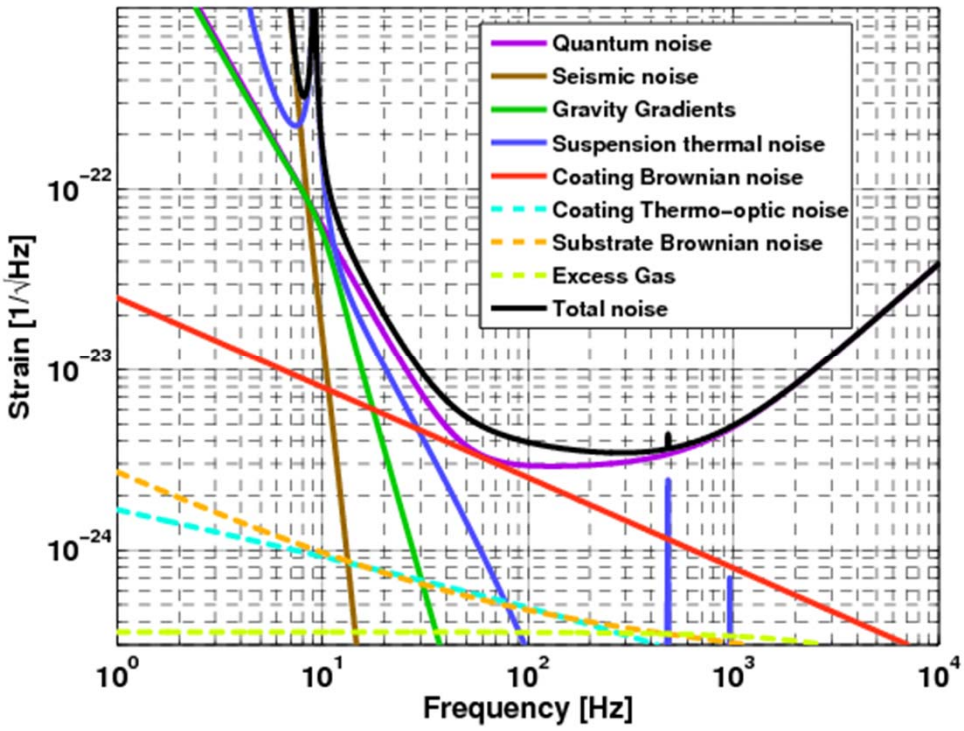

Figure 1 – Advanced LIGO noise budget.

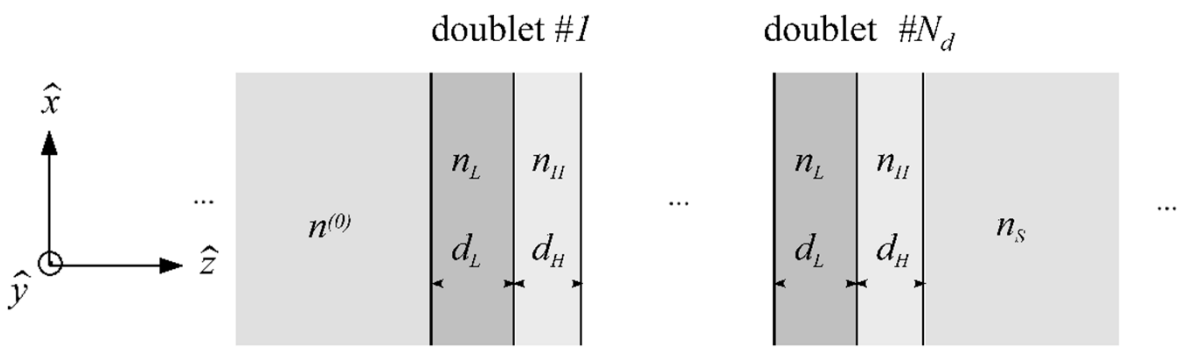

Figure 2 – Stacked – doublet coating geometry, showing the relevant notation for the layer thicknesses and refractionn indexes

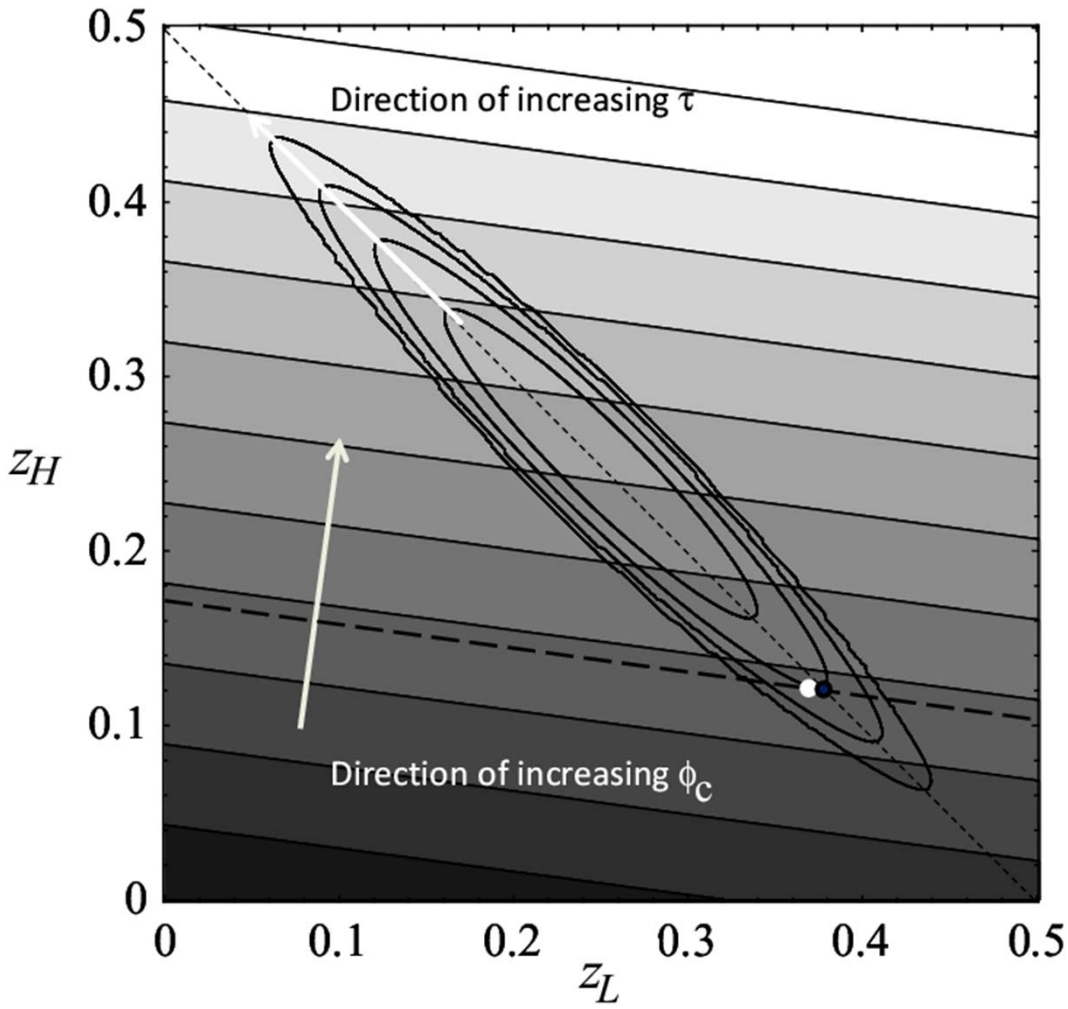

Figure 3 – Contours of constant reflectance and contours of constant Brownian noise in a 5 - doublets coating, as functions of the optical thickness of the low and high index layers.

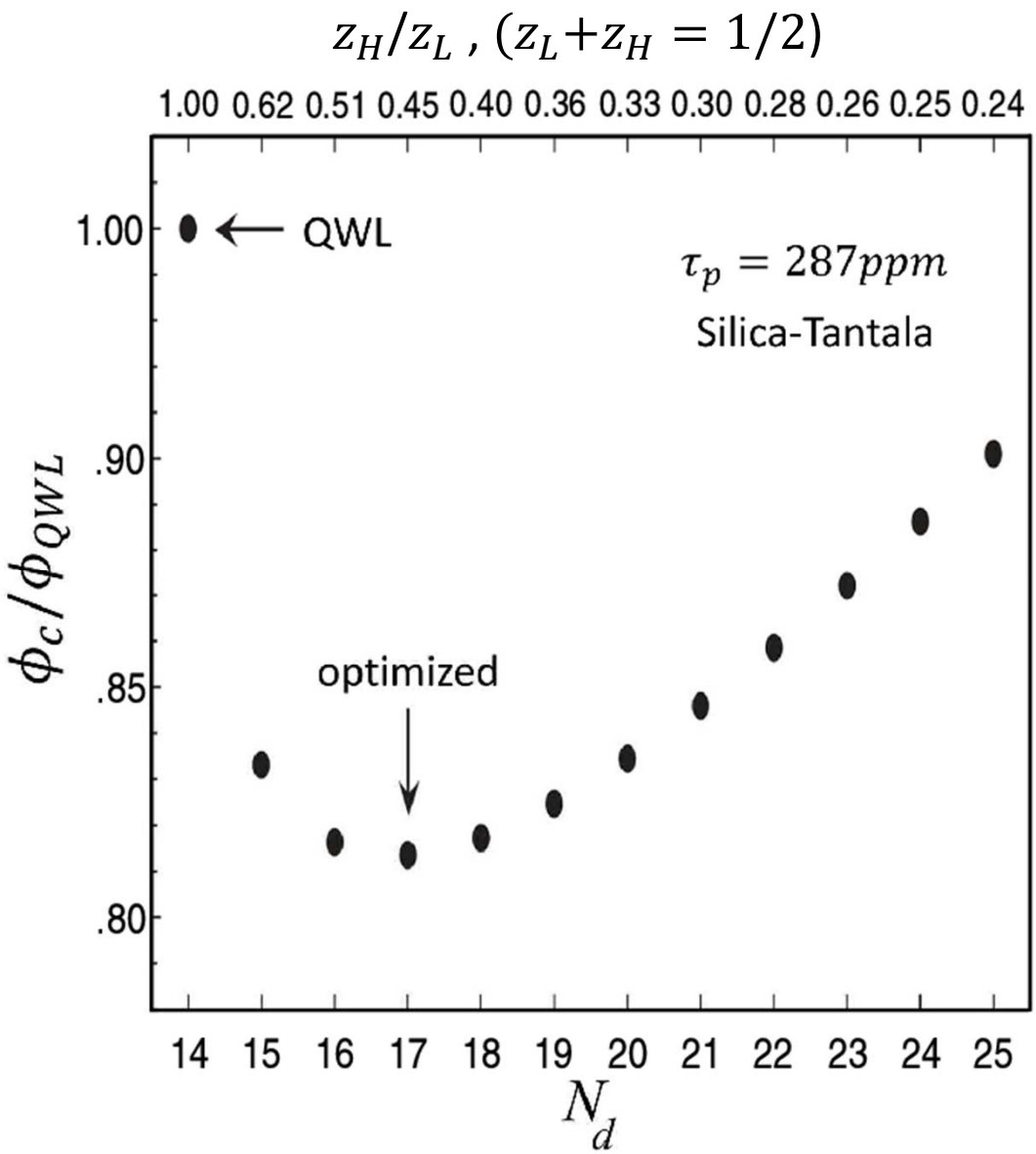

Figure 4 – Coating loss angle of iso - reflective coatings consisting of a different number of Bragg doublets, with different thickness ratios z_H/z_L.

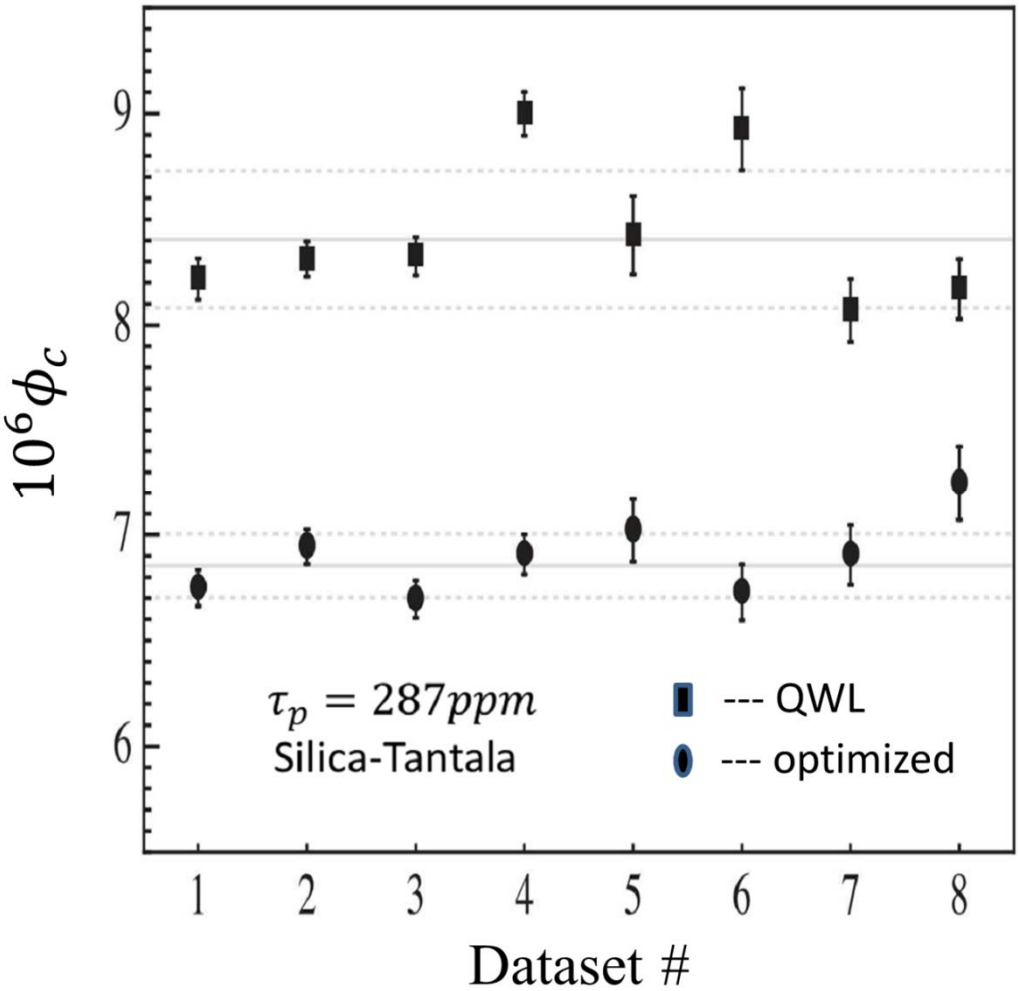

Figure 5 – Coating loss angle of QWL and optimized coating measured at TNI (A. Villar et al., 2010)

$$z_L = 1/4 + \xi_L; z_H = 1/4 - \xi_H$$

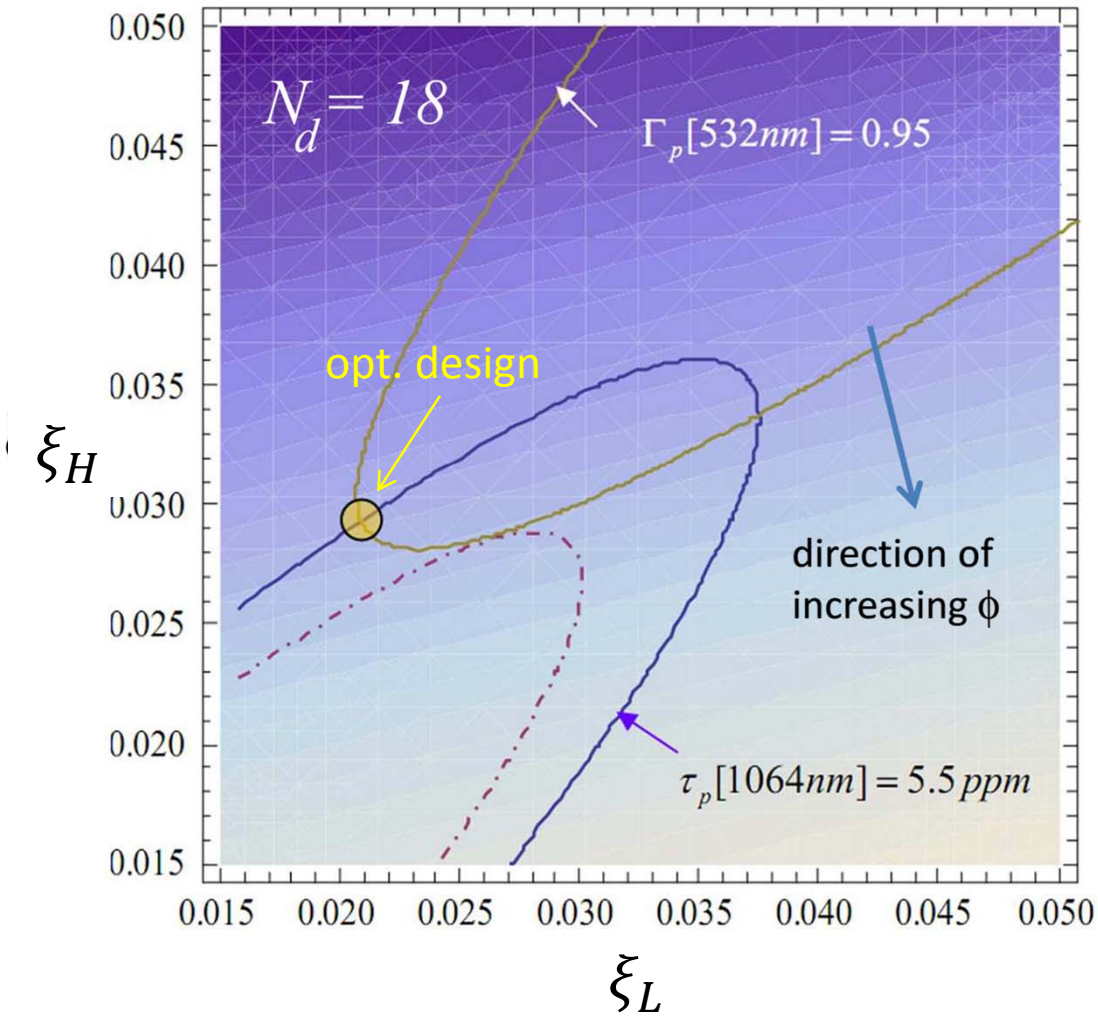

Figure 6 – Stacked doublet dichroic mirror. Constant reflectance contours and constant noise density vs. doublet thickness (M. Principe et al., LIGO G1000380).